PHILOSOPHICAL TRANSACTIONS A

royalsocietypublishing.org/journal/rsta

Research

Cite this article: Maier F, Levin I, Gachkivskyi M, Rödenbeck C, Hammer S. 2023 Estimating regional fossil fuel CO_2 concentrations from $^{14}CO_2$ observations: challenges and uncertainties. *Phil. Trans. R. Soc. A* **381**: 20220203.
https://doi.org/10.1098/rsta.2022.0203

Received: 7 October 2022
Accepted: 9 March 2023

One contribution of 10 to a Theo Murphy meeting issue 'Radiocarbon in the Anthropocene'.

Subject Areas:
atmospheric science

Keywords:
fossil fuel CO_2, radiocarbon, $\Delta^{14}CO_2$ background, nuclear $^{14}CO_2$ contamination

Author for correspondence:
Fabian Maier
e-mail: fabian.maier@iup.uni-heidelberg.de

Downloaded from https://royalsocietypublishing.org/ on 10 October 2023

Estimating regional fossil fuel CO_2 concentrations from $^{14}CO_2$ observations: challenges and uncertainties

Fabian Maier[1], Ingeborg Levin[1], Maksym Gachkivskyi[1,2], Christian Rödenbeck[3] and Samuel Hammer[1,2]

[1]Institut für Umweltphysik, Heidelberg University, INF 229, 69120 Heidelberg, Germany
[2]ICOS Central Radiocarbon Laboratory, Heidelberg University, Berliner Strasse 53, 69120 Heidelberg, Germany
[3]Department Biogeochemical Systems, Max Planck Institute for Biogeochemistry, Hans-Knöll-Strasse 10, 07745 Jena, Germany

FM, 0000-0001-7834-4805; CR, 0000-0001-6011-6249

The direct way to estimate the regional fossil fuel CO_2 surplus ($\Delta ffCO_2$) at a station is by measuring the $\Delta^{14}CO_2$ depletion compared with a respective background. However, this approach has several challenges, which are (i) the choice of an appropriate $\Delta^{14}CO_2$ background, (ii) potential contaminations through nuclear $^{14}CO_2$ emissions and (iii) masking of $\Delta ffCO_2$ by ^{14}C-enriched biosphere respiration. Here we evaluate these challenges and estimate potential biases and typical uncertainties of ^{14}C-based $\Delta ffCO_2$ estimates in Europe. We show that Mace Head (MHD), Ireland, is a representative background station for the Integrated Carbon Observation System (ICOS) atmosphere station network. The mean $\Delta ffCO_2$ representativeness bias when using the MHD $\Delta^{14}CO_2$ background for the whole observation network is of order 0.1 ± 0.3 ppm. At ICOS sites, the median nuclear contamination leads to 25% low-biased $\Delta ffCO_2$ estimates if not corrected for. The $\Delta ffCO_2$ masking due to ^{14}C-enriched heterotrophic CO_2 respiration can lead to similar $\Delta ffCO_2$ biases

© 2023 The Authors. Published by the Royal Society under the terms of the Creative Commons Attribution License http://creativecommons.org/licenses/by/4.0/, which permits unrestricted use, provided the original author and source are credited.

THE ROYAL SOCIETY PUBLISHING

as the nuclear contaminations, especially in summer. Our evaluation of all components contributing to the uncertainty of $\Delta ffCO_2$ estimates reveals that, due to the small $ffCO_2$ signals at ICOS stations, almost half of the ^{14}C-based $\Delta ffCO_2$ estimates from integrated samples have an uncertainty that is larger than 50%.

This article is part of the Theo Murphy meeting issue 'Radiocarbon in the Anthropocene'.

royalsocietypublishing.org/journal/rsta *Phil. Trans. R. Soc. A* **381**: 20220203

Downloaded from https://royalsocietypublishing.org/ on 10 October 2023

1. Introduction

Large uncertainties still exist in greenhouse gases budgets to fully understand the causes of their recent atmospheric changes [1]. The atmospheric boundary layer is the natural integrator of ground-level emissions. In conjunction with atmospheric transport models, trace gas observations in the boundary layer can, therefore, be used to estimate emissions or uptake rates of these gases (e.g. [2,3]). Including process-based emission models and inventories further helps to disentangle natural, e.g. climate-driven changes from anthropogenic emissions. However, there still exist large uncertainties in source attribution. Therefore, supplementary measurements, such as isotopic observations, have been added to the monitoring programmes to help distinguish different sources or constrain sink processes. In the case of CO_2, the radioactive isotope radiocarbon (^{14}C) has a prominent role, e.g. in separating fossil (radiocarbon-free) CO_2 emissions from natural carbon fluxes between atmosphere, ocean and continental biosphere.

^{14}C is a particularly useful tracer on regional and continental scales, where anthropogenic emissions from the burning of fossil fuels play an important role in the carbon budget [4–11]. Disentangling the influence of fossil emissions from ecosystem fluxes on the observed CO_2 concentrations over densely populated areas would, on one hand, provide a means to follow the effectiveness of fossil CO_2 emission reduction strategies (e.g. [12]), on the other hand, allows observing, e.g. climate-driven variations and long-term changes in ecosystem functioning directly from the atmosphere [10]. Co-located observations of CO_2 and $\Delta^{14}CO_2$ (for a definition of the $\Delta^{14}CO_2$-notation that is generally used to report atmospheric $^{14}CO_2$ observations, see §2a) over continents and in polluted areas can be exploited in two ways. One possibility is to derive $\Delta ffCO_2$ estimates from the atmospheric $\Delta^{14}CO_2$ differences between a background site and the (polluted) monitoring station in what we call here the regional isotope budget approach. Alternatively, the CO_2 and $\Delta^{14}CO_2$ observations can be used in a dual-tracer atmospheric inverse modelling framework to estimate the $ffCO_2$ emissions directly [8,10].

The regional isotope budget approach is frequently used to estimate the share of the so-called recently added CO_2 from fossil fuel burning and cement production (e.g. [5,6,13–17]). These studies determined the regional fossil CO_2 excess at an observational station with respect to a non-polluted reference site. This reference or background site could be a high mountain station, which is sampling air from the free troposphere, or a marine site located at the boundary of a continent. The regional isotope budget approach provides the fossil CO_2 excess concentration ($\Delta ffCO_2$, which for clarity we will name C_{ff} in all equations and figures) directly, without the need to model the complete CO_2 and $^{14}CO_2$ cycles. For sites with a long-term $\Delta^{14}CO_2$ record, this approach can also be used to investigate $ffCO_2$ emission trends under the assumption that the atmospheric transport had no significant trend during the considered time period [12].

Typically, however, the $\Delta ffCO_2$ estimates at an observation station show large variations not only on long but also on sub-seasonal time scales, which are mainly driven by atmospheric transport and mixing processes. If this variability can be represented by atmospheric transport models, the $\Delta ffCO_2$ observations can be used in inverse modelling frameworks to estimate the $ffCO_2$ emissions in the footprint of the station [18]. By contrast, the dual-tracer inversion framework [8,10,11] allows for direct usage of the CO_2 and $\Delta^{14}CO_2$ observations to estimate the $ffCO_2$ emissions. But in this alternative approach *a priori* information is needed to represent the CO_2 fluxes from the ocean and the terrestrial biosphere as well as their respective isotopic $^{14}CO_2$

Downloaded from https://royalsocietypublishing.org/ on 10 October 2023

signatures. Furthermore, a representation of the atmospheric $\Delta^{13}CO_2$ signature is required and the cosmogenic production of $^{14}CO_2$ in the upper atmosphere and its (seasonal) transport into the troposphere must be implemented correctly.

Both, the regional isotope budget, and the dual-tracer inversion approach have, thus, advantages and disadvantages. While the dual-tracer inversion requires an *a priori* representation of the CO_2 and $^{14}CO_2$ fluxes and the related atmospheric gradients to directly estimate $ffCO_2$ emissions, the regional isotope budget approach effectively assumes that these can be adequately captured by the appropriate selection of a representative background. Still, both approaches are not always straightforward to apply. In populated areas, we need to consider $^{14}CO_2$ emissions, e.g. from nuclear installations, that contaminate the $\Delta^{14}CO_2$ observations if such emitters are located in the footprints of the sites. Also, CO_2 respired from decomposing organic material, e.g. in soils can mask part of the fossil signal. The biosphere had incorporated bomb ^{14}C in the decades following the atmospheric nuclear bomb testing during the last century, and this $^{14}CO_2$ is today released by heterotrophic respiration [19–21]. While these contaminating $^{14}CO_2$ fluxes must be implemented in the dual-tracer inversion, the regional isotope budget approach uses estimates of correction terms to adjust the observed $\Delta^{14}CO_2$ gradients regarding these masking effects. These correction terms are either based on expert judgement or estimated by simulating the $\Delta^{14}CO_2$ contaminations with *a priori* fluxes and transport models.

Over the years, different assumptions have been made when applying the regional isotope budget approach to, e.g. account for the masking effects mentioned above. The aim of the present study is to in-depth re-visit the regional isotope budget approach, its underlying assumptions and investigate potential biases introduced in the respective results. We make sensitivity analyses to estimate the error contributions from all relevant components in this approach, including effects related to the choice of the background station. To obtain typical estimates of these potential biases and errors, we use the highly populated European continent as target region as this area has established a dense network of $\Delta^{14}CO_2$ observations to validate fossil CO_2 emissions and follow its potential changes [22,23].

2. Methods

(a) The regional isotope budget approach to calculate recently added $ffCO_2$

In the regional isotope budget approach, the CO_2 concentration C_{meas} observed at a measurement station can be written as the sum of the background CO_2 concentration C_{bg} and the recently added or removed CO_2 contributions from different sources and sinks (e.g. [5,6]):

$$C_{meas} = C_{bg} + C_{ff} + C_{resp} + C_{photo}\ (+C_{ocean} + C_{strato}). \tag{2.1}$$

The contribution from the background C_{bg} accounts for the by far largest share and is globally increasing due to global anthropogenic emissions and land use change. The regionally added or removed CO_2 contributions originate from the combustion of fossil fuels and cement production (C_{ff}), the biosphere respiration (C_{resp}) and photosynthesis uptake (C_{photo}) in the target area. It may also contain a component from coastal ocean areas (C_{ocean}) and may be influenced by air mass intrusions from the stratosphere (C_{strato}). Each CO_2 component in equation (2.1) is associated with a characteristic $^{14}CO_2$ signature. When expressing these $^{14}CO_2$ signatures in the so-called Δ-notation, i.e. the relative deviation of the $^{14}C/C$ isotopic ratios from a standard material in permil (as introduced by Stuiver & Pollach [24]), the $\Delta^{14}C$ signatures of the different components are directly comparable, since the Δ-notation accounts for mass-dependent isotopic fractionation during the different exchange processes between the corresponding reservoirs and the atmosphere and also corrects for radioactive decay between sampling and analysis times. Note that, in the following, we replace $\Delta^{14}C$ by Δ^{14} to improve the readability of the equations below.

Downloaded from https://royalsocietypublishing.org/ on 10 October 2023

Since the sum over the products of the individual CO_2 contributions and the associated isotopic signatures $\sum_i C_i \cdot \Delta_i^{14}$ is a conserved quantity [25], it follows that (see [6]):

$$\begin{aligned} C_{meas} \cdot \Delta^{14}_{meas} = {} & C_{bg} \cdot \Delta^{14}_{bg} + C_{ff} \cdot \Delta^{14}_{ff} + C_{resp} \cdot \Delta^{14}_{resp} \\ & + C_{photo} \cdot \Delta^{14}_{photo} (+C_{ocean} \cdot \Delta^{14}_{ocean} + C_{strato} \cdot \Delta^{14}_{strato}) \\ & + C_{meas} \cdot \Delta^{14}_{nuc}. \end{aligned} \tag{2.2}$$

The last term in equation (2.2) considers the potential contamination of the Δ^{14}_{meas} signature at the measurement site by $^{14}CO_2$ emissions from nuclear facilities. These pure $^{14}CO_2$ emissions cause a change in the measured $\Delta^{14}CO_2$ (Δ^{14}_{nuc}) at the station but no change in the observed CO_2 concentration. For European stations the Integrated Carbon Observation System (ICOS) Carbon Portal (CP) provides a dedicated Jupyter notebook to calculate the contamination from nuclear facilities in Europe (freely available after registration at: https://www.icos-cp.eu/data-services/tools/jupyter-notebook, last access: 5 October 2022). With this Jupyter notebook the 3-hourly footprints from each ICOS station can be mapped with the annual mean $^{14}CO_2$ emissions of the European nuclear facilities taken from the Radioactive Discharges Database (RADD). Hence, we use this Jupyter notebook to model for each $\Delta^{14}CO_2$ sample an individual Δ^{14}_{nuc} contribution. The used footprints were calculated with the Stochastic Time-Inverted Lagrangian Transport (STILT, [26]) model. Note that the influence from these (elevated) point sources requires an additional modelling effort if the nuclear installation is located at a distance smaller than *ca* 50 km from the measurement site as shown by Maier *et al*. [27]. This modification has, however, not yet been implemented in the ICOS CP tool. We assume for the modelled Δ^{14}_{nuc} contributions an uncertainty of 100% to account for possible time-dependent (sub-annual) variations in the nuclear $^{14}CO_2$ emissions as well as transport uncertainties. A brief description of how the nuclear $^{14}CO_2$ contributions Δ^{14}_{nuc} are calculated and a more detailed explanation of their assumed uncertainty is given in appendix A.1. The regional isotope budget approach assumes that the background station contains all nuclear contributions from outside the target area and that contaminations from nuclear facilities inside the target area are negligibly small at the background station. This assumption should be appropriate if we use a background site at which only marine air is sampled.

In the further evaluations, we neglect the contributions from (i) the ocean and (ii) the stratosphere, because of the following reasons: (i) In Europe we mainly focus on continental measurement stations without direct oceanic influence. Therefore, we assume that the oceanic CO_2 contribution and its Δ^{14} signature are integrated in the background measurements. This assumption should be appropriate if we use a marine background station; and (ii) we further assume that the latitudinal and vertical differences between the measurement site and the background station are small enough, so that both stations are similarly influenced by ^{14}C-enriched stratospheric air; therefore, we assumed that also the stratospheric component is already integrated in the background measurements. Note that longitudinal differences in the stratospheric ^{14}C production and corresponding influence on tropospheric $\Delta^{14}C$ can be neglected (e.g. [28]).

As the $^{14}C/C$ ratio of fossil CO_2 is zero, the Δ^{14}_{ff} signature of fossil fuel combustion CO_2 is $-1000‰$. Therefore, equation (2.2) can directly be used to calculate the regionally added $ffCO_2$ contribution C_{ff} if all other CO_2 contributions and Δ^{14} signatures are known. However, as the two biospheric CO_2 components, C_{photo} and C_{resp}, are typically not known separately, it is convenient to use equation (2.1) for eliminating the (potentially poorest known) CO_2 contribution from photosynthesis C_{photo} in equation (2.2). As the Δ-notation accounts for mass-dependent isotopic fractionation, we can directly use the Δ^{14} signature of the photosynthesized atmospheric CO_2 to substitute the Δ^{14}_{photo} in equation (2.2). However, the Δ^{14} signature of an air mass changes on its path from the background station to the measurement site and therewith also the Δ^{14} signature taken up by photosynthesis (Δ^{14}_{photo}). Previous studies have either approximated the Δ^{14}_{photo} signature of the photosynthetically absorbed CO_2 with Δ^{14}_{bg} or with Δ^{14}_{meas}. If Δ^{14}_{photo}

Downloaded from https://royalsocietypublishing.org/ on 10 October 2023

is approximated by the Δ^{14}_{meas} value of the ambient CO_2, the $ffCO_2$ excess can be calculated according to:

$$C_{ff} = C_{bg} \cdot \frac{\Delta^{14}_{bg} - \Delta^{14}_{meas}}{\Delta^{14}_{meas} + 1000‰} + C_{meas} \cdot \frac{\Delta^{14}_{nuc}}{\Delta^{14}_{meas} + 1000‰} + C_{resp} \cdot \frac{\Delta^{14}_{resp} - \Delta^{14}_{meas}}{\Delta^{14}_{meas} + 1000‰}. \quad (2.3)$$

Otherwise, if Δ^{14}_{photo} is approximated with the background Δ^{14}_{bg} signature, one gets:

$$C_{ff} = C_{meas} \cdot \frac{\Delta^{14}_{bg} - \Delta^{14}_{meas}}{\Delta^{14}_{bg} + 1000‰} + C_{meas} \cdot \frac{\Delta^{14}_{nuc}}{\Delta^{14}_{bg} + 1000‰} + C_{resp} \cdot \frac{\Delta^{14}_{resp} - \Delta^{14}_{bg}}{\Delta^{14}_{bg} + 1000‰}. \quad (2.4)$$

Which of the approximations, equation (2.3) or (2.4), better estimates regional $\Delta ffCO_2$ depends on how representative the respective Δ^{14}_{photo} approximation is for the biosphere affecting the measurement site. Equation (2.3), for example, is suitable for remote stations that are significantly influenced by the local biosphere. Therefore, the Δ^{14}_{photo} signature of the (mainly contributing) local biosphere is best approximated by the measured Δ^{14}_{meas} signature of the ambient air CO_2 at the measurement site. By contrast, equation (2.4) might be applicable for stations with very little influence of the local biosphere and supposedly large local fossil emissions. Thus, it might be less appropriate to approximate the Δ^{14}_{photo} signature of the photosynthetically absorbed air with the strongly depleted ambient air Δ^{14}_{meas} signature. Indeed, for such cases the Δ^{14}_{bg} signature might more accurately describe the Δ^{14}_{photo} signature of the (mainly contributing) far field biosphere. The difference between using the two alternative equations will be evaluated in §3a(i).

(b) Importance of the components and correction terms in the regional isotope budget approach for estimating $\Delta ffCO_2$

The choice of the background station is crucial for the $\Delta ffCO_2$ estimate, since the first term in equations (2.3) and (2.4) is proportional to the Δ^{14} difference between the measurement station and the background station and usually contributes the most. Ideally, a single site can be used to provide a physically representative background for all other observation sites within a $\Delta^{14}CO_2$ monitoring network. This will be the case when all observation sites within the sampling domain are influenced by the same weather systems, generally flowing from the background to the observation sites. In the modelling world, this would mean that the unique background should be valid for all boundaries of the targeted domain, for which the $ffCO_2$ flux shall be estimated. This assumption of representativeness is examined further in §3a(ii).

The second term in equations (2.3) and (2.4) describes the corrections for nuclear contaminations at the measurement site. Particularly in Europe with many nuclear power plants and two large nuclear fuel reprocessing plants (cf. figure 8), disregarding these nuclear contaminations would result in significant underestimation of $\Delta ffCO_2$ estimates [5,29,30].

The third term in equations (2.3) and (2.4) accounts for the correction for biosphere respiration, which, if not accounted for, may also mask part of the $\Delta ffCO_2$. The Δ^{14}_{resp} signature differs for autotrophic and heterotrophic respiration. In earlier studies (e.g. [13]), we approximated the autotrophic Δ^{14}_{resp} signature with that of background air, while for the heterotrophic component, we used the $\Delta^{14}C$ signature modelled by Naegler & Levin [31]. Turnbull *et al*. [6] assumed a mean terrestrial carbon residence time of 10 ± 10 years and used the ^{14}C history of the Northern Hemisphere to calculate the Δ^{14} signature of heterotrophic respiration. Δ^{14}_{soil} of soil respiration was measured in summer 2012 at a boreal forest site in Finland by Palonen *et al*. [32] to lie between (48.2–56.7)‰, values about 20‰ higher than background air in that year. Chanca [33] reported a mean Δ^{14}_{resp} of 32.0 ± 7.4‰ for a tropical rainforest site in Brazil. This latter value was on average 29‰ higher than atmospheric CO_2 in that year. From these studies, we conclude that Δ^{14}_{resp} in the last decade was a few tens of ‰ higher than the contemporary atmospheric CO_2. We used the Vegetation Photosynthesis and Respiration Model (VPRM, [34]) in combination with

Downloaded from https://royalsocietypublishing.org/ on 10 October 2023

STILT to simulate the respiration CO_2 signal C_{resp} for the two ICOS sites Observatoire Pérenne de l'Environnement (OPE) in France and Křešín (KRE) in the Czech Republic. These results show on average about twice as high C_{resp} signals in summer than in winter. Overall, we would expect the typical range of C_{resp} to be between 2 and 8 ppm at ICOS sites in Central Europe.

3. Results

The aim of the present study is to quantify potential biases and estimate individual error contributions to the total uncertainty of $\Delta ffCO_2$ resulting from the uncertainties of the measured and estimated parameters and corrections in equations (2.3) and (2.4). In §3a, we first evaluate the difference of results when approximating Δ^{14}_{photo} by Δ^{14}_{meas} or Δ^{14}_{bg}, respectively. Then, as a typical example for a populated region, we evaluate biases introduced in the $\Delta ffCO_2$ result when selecting only a single background station for Europe that is located on the western coast of Ireland. We will further quantify the biases in the $\Delta ffCO_2$ estimates, which would be induced when ignoring nuclear contaminations, and finally, we investigate the bias related to $\Delta^{14}C$-enriched respiration CO_2. Section 3b investigates the relative uncertainty contributions introduced through (i) the uncertainty of the CO_2 and $\Delta^{14}CO_2$ observations at the measurement station, (ii) the uncertainty of the background $\Delta^{14}CO_2$ curve, which incorporates the uncertainty of its construction (smooth curve fitted through observational data at that background station) as well as the uncertainty due to the representativeness of the background curve. We will (iii) estimate the uncertainty of the correction for nuclear $^{14}CO_2$ contamination and (iv) the error contribution of the correction for heterotrophic respiration. Finally, we assess the total uncertainty of typical (bias-corrected) $\Delta ffCO_2$ estimates at European ICOS stations by identifying those components/parameters with the largest impact.

(a) Potential bias components in the $\Delta ffCO_2$ estimates

(i) Bias due to the approximation of Δ^{14}_{photo} (choice of equation (2.3) or (2.4))

To investigate the impact of the approximation of Δ^{14}_{photo} on the $\Delta ffCO_2$ estimates, i.e. the difference between equation (2.3) and (2.4), figure 1 shows the ratio of the $\Delta ffCO_2$ results from equation (2.4) to (2.3) plotted versus the $(\Delta^{14}_{bg} - \Delta^{14}_{meas})$ difference for typical current $\Delta^{14}CO_2$ and CO_2 values (cf. table 1) and a large range of possible ratios of C_{photo} to C_{ff}. As can be seen from figure 1, the differences in the final $\Delta ffCO_2$ results when using equation (2.4) versus (2.3) can be large at stations where the (negative) photosynthetic component is much larger than the (positive) $\Delta ffCO_2$ component and if the $\Delta^{14}CO_2$ difference between station and background is large. Typical $(\Delta^{14}_{bg} - \Delta^{14}_{meas})$ differences at ICOS stations go up to 10‰ (cf. figure 6 below), and in cases with high differences (large $\Delta ffCO_2$), i.e. in winter, the photosynthetic uptake is generally small, so that we expect $|C_{photo}/C_{ff}|$ ratios < 2 (figure 9). Therefore, we expect biases between using equation (2.3) relative to equation (2.4) to be restricted to a few per cent only. In summer, the $|C_{photo}/C_{ff}|$ ratio is larger but the $\Delta^{14}CO_2$ difference to the background tends to be smaller, again pushing the difference between the equations into the range of few per cent. As we are evaluating here typical biases and uncertainties of ^{14}C-based $\Delta ffCO_2$ at ICOS stations that are typically located more than 40 km away from large $ffCO_2$ emitting regions [35], the photosynthetic uptake signals will most probably be larger than those from fossil emissions (figure 9). Therefore, we restrict our further analysis on $\Delta ffCO_2$ estimates applying equation (2.3).

(ii) Biases due to the choice of one background station

Representation of background air with respect to individual ICOS stations: The regional isotope budget approach estimates $\Delta ffCO_2$ with respect to a (measured) background. It implicitly assumes that the air masses arriving at the stations started with this background value. In order to use the $\Delta ffCO_2$ estimates to obtain information on fossil emissions in a given target area, it

Downloaded from https://royalsocietypublishing.org/ on 10 October 2023

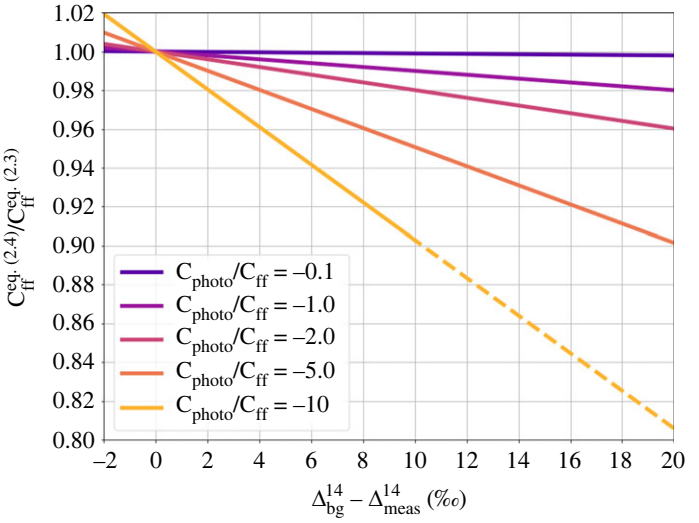

Figure 1. Ratio of $\Delta ffCO_2$ when estimated with equation (2.4) versus equation (2.3) for C_{photo}/C_{ff} ratios ranging from −0.1 to −10.

Table 1. Assumed values and parameters for our standard uncertainty evaluation.

parameter	value ± uncertainty	description
C_{meas}	(420 ± 0.1) ppm	CO_2 concentration at station
Δ^{14}_{meas}	±2‰	typical $\Delta^{14}CO_2$ measurement uncertainty
C_{bg}	(410 ± 1) ppm	background CO_2 concentration
Δ^{14}_{bg}	(3 ± 1)‰	taken from fitted background curve of MHD data
Δ^{14}_{nuc}	(1 ± 1)‰	typical nuclear $\Delta^{14}CO_2$ contamination at ICOS stations
C_{resp}/C_{ff}	3 ± 3	respiration CO_2 component relative to $\Delta ffCO_2$
Δ^{14}_{resp}	(25 ± 12)‰	respiration $\Delta^{14}CO_2$ signature

is necessary to assess the implicit assumption that the selected background is representative of all boundaries of this target area. We examine the representativeness problem using Europe and the ICOS observation network as an example target area. We base our evaluation on the standard STILT domain over Europe, which extends from 33° N to 73° N and from 15° W to 35° E (figure 2). The distribution of the typical air mass origins entering the STILT domain is constructed by the endpoints of hourly 10-days STILT back-trajectories for the year 2018 for nine ICOS stations, where regular $\Delta^{14}CO_2$ observations are conducted. The abundance distributions of those trajectory endpoints at the four boundaries (figure 2) clearly indicate that these central European stations are predominantly influenced by westerly winds, which transport Atlantic air masses to the European continent. On average, 67% of the back-trajectories from the ICOS sites end at (or go beyond) the western boundary of the model domain, with an accumulation between roughly 45° and 60° N. This is a good argument to select Mace Head (MHD, 53.33° N, 9.90° W, 5 m a.s.l.), located close to the western boundary of the STILT domain, as a background site to calculate the $ffCO_2$ excess at European (ICOS) stations. MHD is located on the west coast of Ireland and atmospheric $^{14}CO_2$ samples are only collected during situations when the air comes from the marine sector. These $\Delta^{14}CO_2$ (together with CO_2) background measurements can thus be assumed as representative for the Atlantic boundary of the European continent. However, they

Downloaded from https://royalsocietypublishing.org/ on 10 October 2023

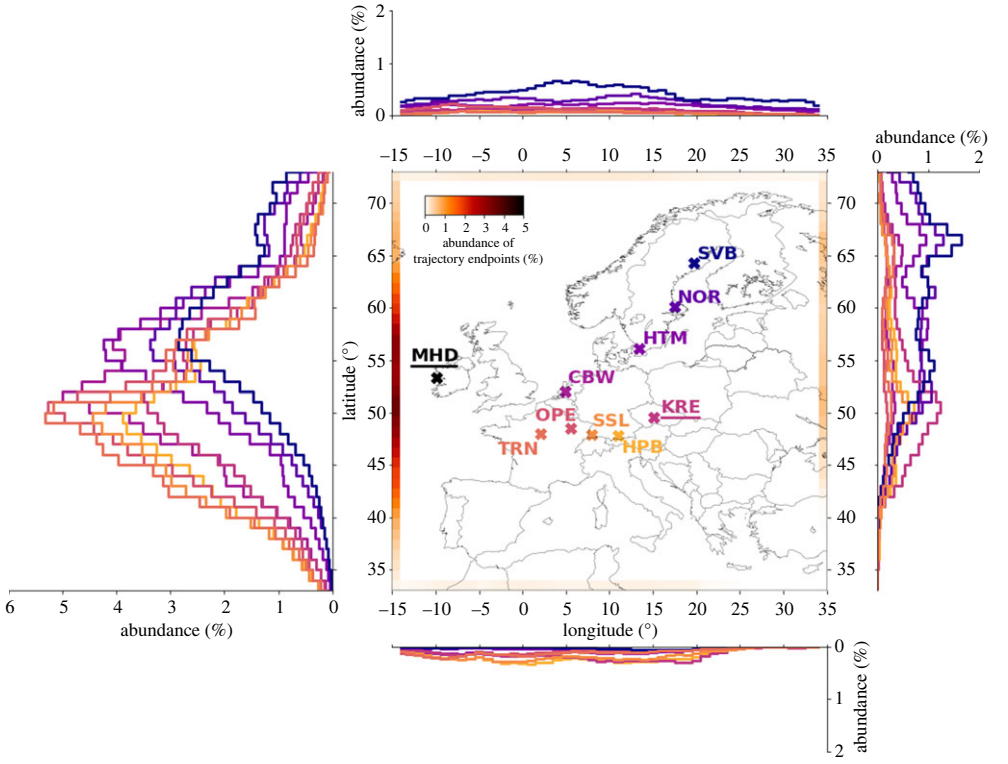

Figure 2. Abundance distribution for the endpoints of the STILT back-trajectories from nine ICOS sites (coloured crosses) in 2018. At each hour and each station, 100 particles were released in STILT, and their back-trajectories were calculated for 10 days backward in time. If the trajectory leaves the shown domain, its endpoint is defined as the grid cell where the trajectory leaves the domain the first time. STILT was driven with the 0.25° resolved ERA5 (European ReAnalysis 5) meteorology from the European Center for Medium-Range Weather Forecasts (ECMWF). The black cross indicates the position of the Mace Head (MHD) background site (back-trajectories were not calculated for MHD).

may be less suitable as background reference in situations when the measurement stations are influenced by easterly (or southerly) air masses, which transport potentially polluted continental air to our domain. Also northerly Arctic air masses may have a different $\Delta^{14}CO_2$ level. Figure 2 shows that for on average 33% of the time in 2018 the air masses originated from non-western boundaries (or from within the target area) with on average 13% of all situations in 2018 entering via the eastern boundary.

Background variability at boundaries of the target area: Currently, no background $\Delta^{14}CO_2$ observations exist in eastern Europe or close to the eastern boundary of our target domain. This makes it impossible to construct a purely observation-based $\Delta^{14}CO_2$ reference for the eastern air masses entering our target region and to deduce the bias of the representativeness problem from this. Therefore, we used the global atmospheric tracer transport model TM3 ([36]; spatial resolution of 4° × 5°) to estimate $ffCO_2$ concentrations of air masses entering the eastern boundary of our domain. For this simulation, $ffCO_2$ emissions within the European target domain have been set to zero, while we used the Global Carbon Budget Gridded Fossil Emissions Dataset (GCP-GridFED; v.2022.2) emissions [37] elsewhere. Figure 3*a*,*b* shows the simulated $ffCO_2$ concentration difference of hourly data (purple dots) between a virtual station located at the eastern boundary of the STILT domain at mid-latitudes (55° N, 34° E, 150 m a.g.l.) and MHD for the years 2016–2020. As expected, this difference is generally positive. It varies between a few tenths of a ppm up to more than 8 ppm in one event in 2020. A significant seasonal variation is observed, with higher concentration differences compared with MHD during winter and lower differences in summer.

Downloaded from https://royalsocietypublishing.org/ on 10 October 2023

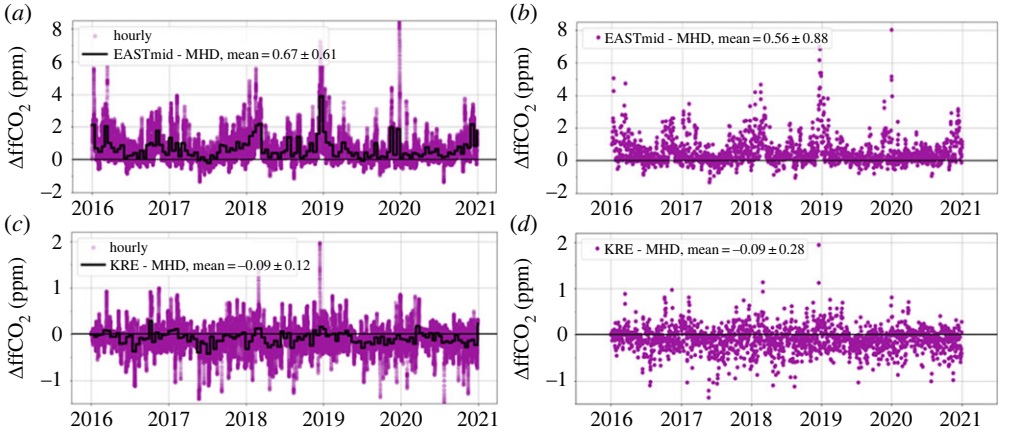

Figure 3. TM3-simulated fossil fuel CO_2 concentration offsets relative to Mace Head caused by emissions outside of our target region (figure 2). (*a*,*b*) The offsets at a location at mid-latitudes of the eastern boundary, for all hours (*a*) and for 13 h UTC only (*b*). (*c*,*d*) Corresponding data for the ICOS station Křešín (KRE). Note the different scales in (*a*,*b*) and (*c*,*d*).

This seasonality is mainly due to seasonal variations of emissions, but also due to seasonal variations in atmospheric transport. As emissions within the target domain were set to zero in this TM3 model run, the concentration differences in figure 3*a*,*b* provide a good approximation of the $ffCO_2$ concentration offset (relative to MHD) of air masses entering the domain from the east. Figure 3*a* shows the biases for all hours in 2016–2020 and for averages of two-week integrated samples (black solid line). Figure 3*b* shows the difference for potential flask samples collected at midday. For any potential station located close to this border, this difference would represent the approximate positive bias of the calculated $\Delta ffCO_2$ for those situations when the station is *not* influenced by westerly air masses but by air from the east. The mean bias is about 20% larger for all hours and two-week integrated samples than for flask samples collected at midday. For flask samples, however, the standard deviation of that bias is about 30% higher than for two-week integrated samples since flask samples depend stronger on individual weather situations. The station in the ICOS network located closest to the eastern border of the target domain is Křešín (KRE). This station typically experiences about 16% of situations with easterly trajectories (figure 2). On average over *all* situations of potential flasks sampled at Křešín at midday, the $\Delta ffCO_2$ bias would thus be only $0.56 \times 0.16 = 0.09$ ppm. However, Křešín station is located about 20° west of the eastern boundary. Therefore, any contribution from domain-external $ffCO_2$ emissions coming from the east will be diluted during transport of the air mass to the station.

We can use similar arguments and the TM3 model results to estimate the influence on ICOS stations due to emissions from outside our domain from the west, e.g. from North America. The concentration from such sources as observed at MHD would also be (further) diluted when the air mass travels over Europe and reaches, e.g. the Křešín station. This is why in figure 3*c*,*d*, where we plot the difference of the TM3 concentrations simulated for KRE minus those at MHD, often turn out to be negative. Note that the positive values in this plot are the signals from the easterly trajectories, but here diluted during the transport from the eastern boundary to the Křešín site. As the majority of trajectories reaching Křešín comes from the west, the average difference is negative. In summary, we expect typical mean representativeness biases of order (0.1 ± 0.3) ppm $\Delta ffCO_2$ when applying the regional isotope budget approach for the investigated example of the ICOS station network with MHD as a background in the STILT domain. A $ffCO_2$ inversion using our $\Delta ffCO_2$ estimates would incorrectly locate this (0.1 ± 0.3) ppm representativeness bias within the STILT domain.

Downloaded from https://royalsocietypublishing.org/ on 10 October 2023

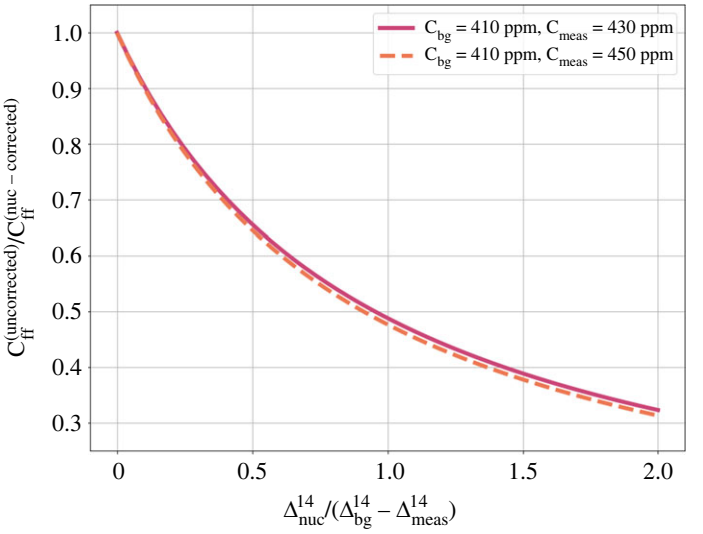

Figure 4. $\Delta ffCO_2$ masking by $^{14}CO_2$ emissions from nuclear installations in relation to the ratio between Δ^{14}_{nuc} and $(\Delta^{14}_{bg} - \Delta^{14}_{meas})$.

Influence of a latitudinal $\Delta^{14}CO_2$ *gradient:* The MHD background station is located at about 55° N, a latitude where global fossil CO_2 emissions are large. We would, thus, expect lower fossil CO_2 concentrations at lower latitudes of the Northern Hemisphere, corresponding to slightly higher $\Delta^{14}CO_2$ in background air further south. Levin *et al*. [38] published mean $\Delta^{14}CO_2$ data from Izaña station on Tenerife Island (28.3° N, 16.48° W, 2373 m a.s.l.) in the Atlantic Ocean, which indeed showed slightly higher values in the 1990s. However, in the last decade, the $\Delta^{14}CO_2$ difference to MHD is smaller than 1‰. As air masses only occasionally arrive from latitudes south of 40° N, the potential bias due to a latitudinal $\Delta^{14}CO_2$ gradient is assumed negligible and thus not taken into account here as a potential bias.

(iii) Biases due to nuclear $^{14}CO_2$ emissions

As mentioned before, $^{14}CO_2$ contaminations by emissions from nuclear installations are a potentially serious problem for ^{14}C-based $\Delta ffCO_2$ estimates in Europe ([29,30]; figure 8 for a distribution of the nuclear $^{14}CO_2$ emissions in Europe). This may be particularly true at stations with small $\Delta ffCO_2$ signals, i.e. small $\Delta^{14}CO_2$ depletion at the measurement station compared with the background $(\Delta^{14}_{bg} - \Delta^{14}_{meas})$. We, therefore, estimated the masking of $\Delta ffCO_2$ $(C_{ff}^{uncorrected}/C_{ff}^{nuc\text{ - }corrected})$ with respect to the ratio between Δ^{14}_{nuc} and $(\Delta^{14}_{bg} - \Delta^{14}_{meas})$. As this masking effect (second term in equation (2.3)) also depends on the CO_2 concentration at the measurement station, we estimated the masking for two typical concentrations, $C_{meas} = 430$ and 450 ppm, respectively, as displayed in figure 4.

A relative Δ^{14}_{nuc} contamination from nuclear emissions of about 25% of the $(\Delta^{14}_{bg} - \Delta^{14}_{meas})$ signal would mask about 20% of the $\Delta ffCO_2$ signal. The nuclear correction is, thus, especially important for stations with small $\Delta^{14}C$-depletions compared with the background site, as indeed expected at ICOS atmosphere stations (see below, figure 6). Sampling during times with potential influence from nuclear installations should, therefore, be avoided, e.g. for flask sampling, or the bias must be calculated precisely (see §3b(iv)).

(iv) Biases due to ^{14}C-enriched biosphere respiration

Also soil respiration can mask part of the fossil fuel-related $\Delta^{14}C$ difference between the stations and the background site. In this case, however, the contaminating source does not emit pure $^{14}CO_2$, as is the case for nuclear installations. The respired CO_2 today, if at all, is only slightly

Downloaded from https://royalsocietypublishing.org/ on 10 October 2023

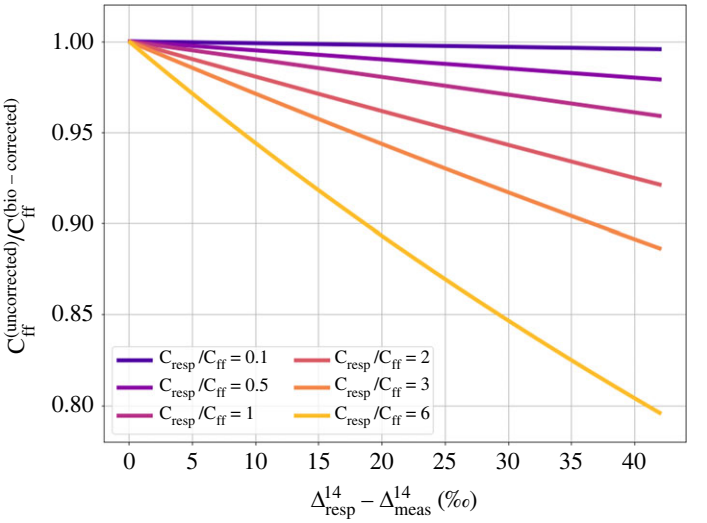

Figure 5. $\Delta ffCO_2$ masking by ^{14}C-enriched respiration CO_2 plotted versus the difference between ($\Delta^{14}_{resp} - \Delta^{14}_{meas}$) for C_{resp}/C_{ff} ratios between 0.1 and 6.

enriched in $\Delta^{14}C$ compared with contemporary ambient CO_2. Unfortunately, only very few measured data are available on Δ^{14}_{resp} in different ecosystems. These data suggest enrichments of a few tens of ‰ compared with atmospheric CO_2 [32,33]. Figure 5 shows the masking of $\Delta ffCO_2$ ($C_{ff}^{uncorrected}/C_{ff}^{bio\text{ - }corrected}$) in relation to the Δ^{14} difference between respired and measured CO_2 ($\Delta^{14}_{resp} - \Delta^{14}_{meas}$) for a range of C_{resp}/C_{ff} ratios between 0.1 and 6.

If the C_{resp} signal has a similar magnitude as $\Delta ffCO_2$ (i.e. $C_{resp}/C_{ff} = 1$), which is a typical ratio in winter (figure 9), the uncorrected $\Delta ffCO_2$ is underestimated by less than 5%, under the assumption that the Δ^{14} difference between respiration CO_2 and measured CO_2 is smaller than 40‰. Apparently, this bias increases with an increasing relative C_{resp} signal. Thus, the biosphere correction is potentially important at stations with low $\Delta ffCO_2$ and a high respiration component C_{resp}, which is the case for a number of ICOS stations in summer and in Northern Europe, i.e. far away from high $ffCO_2$ emission areas. Here we can find C_{resp}/C_{ff} ratios as large as 6 (figure 9). In such situations, the $\Delta ffCO_2$ masking due to ignoring the biosphere correction (third term in equation (2.3)) could become as large as 20%, if the Δ^{14} difference between respiration CO_2 and ambient air CO_2 is larger than 40‰.

(v) Typical $\Delta^{14}CO_2$ signals at ICOS stations

The relevance of the two bias correction terms for nuclear and respiration contamination at ICOS stations discussed above depends on their individual influence areas with respect to fossil emitters and $^{14}CO_2$-emitting nuclear installations. It also depends on the type of samples collected (two-week integrated versus midday flasks). Figure 6*a* shows the distribution of ($\Delta^{14}_{bg} - \Delta^{14}_{meas}$) of two-week integrated samples collected in the years 2017–2020 at the nine ICOS stations shown in figure 1. Figure 6*b* gives the distribution of the mean Δ^{14}_{nuc} contaminations for the same stations and sample type. The median measured $\Delta^{14}CO_2$ difference between station and background (MHD) is only 3.8‰ while the median nuclear contamination amounts to about 30% of that value. If not corrected, this would correspond to an almost 25% masking of $\Delta ffCO_2$. This illustrates the importance of the nuclear contamination problem in Europe and the need to correctly model Δ^{14}_{nuc}. Such a correction could best be done with high-resolution emissions data and a reliable transport modelling system. Currently, however, only annual mean $^{14}CO_2$ emission data are available.

Downloaded from https://royalsocietypublishing.org/ on 10 October 2023

Figure 6*c*,*d* shows similar distributions as *a*,*b*, but for hourly flask samples collected at 13 h local time. The median ($\Delta^{14}_{bg} - \Delta^{14}_{meas}$) difference for the currently available flask samples—yet collected only at seven ICOS class-1 stations—is 4.4‰, slightly larger than for two-week integrated samples, while the nuclear correction term is, on average, only half of that for the integrated samples. Still the average masking of about 15% is significant and should be corrected.

(b) Uncertainty of the $\Delta ffCO_2$ estimates

After having quantified potential biases when using (i) equation (2.4) instead of equation (2.3) to estimate recently added $ffCO_2$, (ii) the potential bias due to the use of a single background station for all European ICOS sites, (iii) neglecting corrections for nuclear $^{14}CO_2$ emissions and (iv) for $\Delta ffCO_2$ masking due to ^{14}C-elevated biosphere respiration, in the following we evaluate the contributions to the total uncertainty of the bias-corrected $\Delta ffCO_2$, including the uncertainty due to these bias corrections.

(i) Typical measurement uncertainty

One important uncertainty contribution to estimate recently added fossil CO_2 is the $\Delta^{14}CO_2$ measurement uncertainty. This uncertainty is relevant for the measurements at the ICOS sites but also for estimating the background reference, here from MHD data. Both determine the uncertainty of the main term in equations (2.3) and (2.4). Typical high-precision radiocarbon laboratories measure single atmospheric $^{14}CO_2$ samples with a precision between $\Delta^{14}C = (1.7–2.3)$‰ (e.g. [39]). This range also covers the average precision and long-term repeatability in the ICOS Radiocarbon Laboratory for integrated and flask samples. For simplicity we assume here a measurement precision of 2‰ for all $\Delta^{14}CO_2$ analyses.

(ii) Uncertainty of the $^{14}CO_2$ background estimate

The uncertainty of the $^{14}CO_2$ background estimate comprises two components. On the one hand, the uncertainties resulting from the construction of the $^{14}CO_2$ background curve from the measurements at the background station, and on the other hand, the uncertainties resulting from the representativeness assumption. As illustrated in §3a(ii), using MHD as single background for all ICOS stations in western and central Europe could lead to a mean $\Delta ffCO_2$ bias of order 0.1 ppm for two-week integrated samples and also for flask samples collected over one hour at midday at the most easterly located station KRE. The standard deviation of this bias was estimated to 0.12 ppm for integrated and to 0.28 ppm for flask samples, with individual biases of up to 2 ppm in exceptional cases. The variability of the bias can be seen as the representativeness uncertainty of the $^{14}CO_2$ background.

To construct a continuous $\Delta^{14}CO_2$ background curve for MHD that is applicable for flask and integrated samples, we calculated a smooth curve through these data by using a curve fitting routine developed by the National Oceanic and Atmospheric Administration (NOAA) [40]. A detailed description of how the background curve has been calculated is given in Appendix A.2. Two different uncertainty estimates have been made for the background reference, one based on the standard NOAA routine and a second one using a Monte Carlo approach. From these estimates we derived a mean uncertainty for Δ^{14}_{bg} of ±0.86‰. Adding the (independent) background representativeness uncertainty mentioned above, we obtain a total background reference uncertainty for integrated samples of 0.9‰ and for flask samples of 1.0‰. The uncertainty of the background CO_2 reference concentration curve is negligible for the overall $\Delta ffCO_2$ uncertainty, even if an assumed upper-limit CO_2 background representativeness uncertainty of 5 ppm is added.

Downloaded from https://royalsocietypublishing.org/ on 10 October 2023

(iii) Uncertainty of the nuclear and respiration masking corrections

In order to estimate the error contributions of the two correction terms in equation (2.3) (masking by nuclear $^{14}CO_2$ emissions, second term, and contribution from respiration of ^{14}C-enriched CO_2, third term), we made the following assumptions: we assume 100% uncertainty for the nuclear contamination estimates; this is justified with a significant transport model error to correctly simulate the dispersion and location of power plant plumes and by the fact that the significant temporal variability of the nuclear emissions (e.g. [30]) is totally ignored when using the currently reported annual mean emissions from RADD for estimating Δ^{14}_{nuc} (see appendix A.1). The $\Delta ffCO_2$ masking contribution from CO_2 respiration, C_{resp}, has also a significant uncertainty because for daytime situations it has to be estimated using, e.g. a vegetation model that is coupled to an atmospheric transport model. For night-time situations when photosynthetic uptake of CO_2 is negligible, C_{resp} or C_{resp}/C_{ff}, the latter being the relevant parameter that determines the masking (cf. figure 5), could be estimated in an iterative way as the difference between C_{meas}, C_{bg} and C_{ff}. Finally, we estimate the uncertainty of Δ^{14}_{resp} to be 50% of the difference between Δ^{14}_{resp} and Δ^{14}_{meas}. This means, if we measure a Δ^{14}_{meas} of 1‰ and assume a Δ^{14}_{resp} signature of 25‰, the applied uncertainty for Δ^{14}_{resp} would be 12‰. The dependence of the Δ^{14}_{resp} uncertainty on the $(\Delta^{14}_{resp} - \Delta^{14}_{meas})$ difference seems appropriate as the biosphere correction (third term in equation (2.3)) is also dependent on the $(\Delta^{14}_{resp} - \Delta^{14}_{meas})$ difference (figure 5).

(iv) Overall uncertainty of $\Delta ffCO_2$ for typical ICOS stations

The assumed concrete values and parameters that were used in the following overall error estimate of $\Delta ffCO_2$ derived from $\Delta^{14}CO_2$ measurements of two-week integrated and flask samples at typical ICOS stations and their assumed uncertainties are listed in table 1. Figure 7*a* shows the relative uncertainty of bias-corrected $\Delta ffCO_2$ in relation to the difference of Δ^{14} between background and station $(\Delta^{14}_{bg} - \Delta^{14}_{meas})$, while figure 7*b* shows the absolute uncertainty in ppm. The different colours show different combinations of individual uncertainty contributions. It is obvious that the largest contribution to the overall uncertainty of bias-corrected $\Delta ffCO_2$ is due to the analytical error of the ^{14}C measurements, Δ^{14}_{meas}. When adding an uncertainty of the background reference Δ^{14}_{bg} of 1‰ and a typical nuclear contamination of $\Delta^{14}_{nuc} = (1 \pm 1)$‰, the overall uncertainty of (bias-corrected) $\Delta ffCO_2$ is larger than 50% at an observed $(\Delta^{14}_{bg} - \Delta^{14}_{meas})$ difference smaller than 3.5‰. (Note that the uncertainty of C_{meas} and C_{bg} have not been added in figure 7 as both error contributions are negligible.) Considering the median $(\Delta^{14}_{bg} - \Delta^{14}_{meas})$ value (figure 6*a*,*b*), this means that, when ignoring the uncertainty due to respiration masking (yellow curve in figure 7), almost half of the ^{14}C-based $\Delta ffCO_2$ estimates from integrated samples at ICOS stations have an uncertainty greater than 50%. Only at observed $(\Delta^{14}_{bg} - \Delta^{14}_{meas})$ differences larger than 8‰ the uncertainty of the $\Delta ffCO_2$ estimate becomes smaller than 25%. This illustrates the importance of precise $\Delta^{14}CO_2$ measurements. If the $\Delta^{14}CO_2$ measurement uncertainty can be reduced to 1‰, only about one-third of the integrated samples at ICOS stations would have an $\Delta ffCO_2$ uncertainty greater than 50%.

Figure 7*b* shows the absolute uncertainty of bias-corrected $\Delta ffCO_2$ in ppm. The absolute error is only slightly increasing to 1.1 ppm (for an assumed 2‰ Δ^{14}_{meas} uncertainty) with larger differences between background reference and station $(\Delta^{14}_{bg} - \Delta^{14}_{meas})$. The yellow curves in figure 7*a*,*b* show the uncertainty contribution from C_{resp}, when assuming that the respiration CO_2 (C_{resp}) signal is three times higher than C_{ff}. During summer, when the $(\Delta^{14}_{bg} - \Delta^{14}_{meas})$ difference is small, the C_{resp}/C_{ff} is often larger than 3 (figure 9); however, in connection with low $(\Delta^{14}_{bg} - \Delta^{14}_{meas})$ differences the error contribution from respiration masking will still be small. Contrary, for situations with high fossil components, i.e. during winter, we expect a ratio of less than 3; therefore, we conclude that an uncertainty contribution of 0.5 ppm due to respiration masking correction, as shown in figure 7*b*, probably represents an upper limit. All-in-all, however,

Downloaded from https://royalsocietypublishing.org/ on 10 October 2023

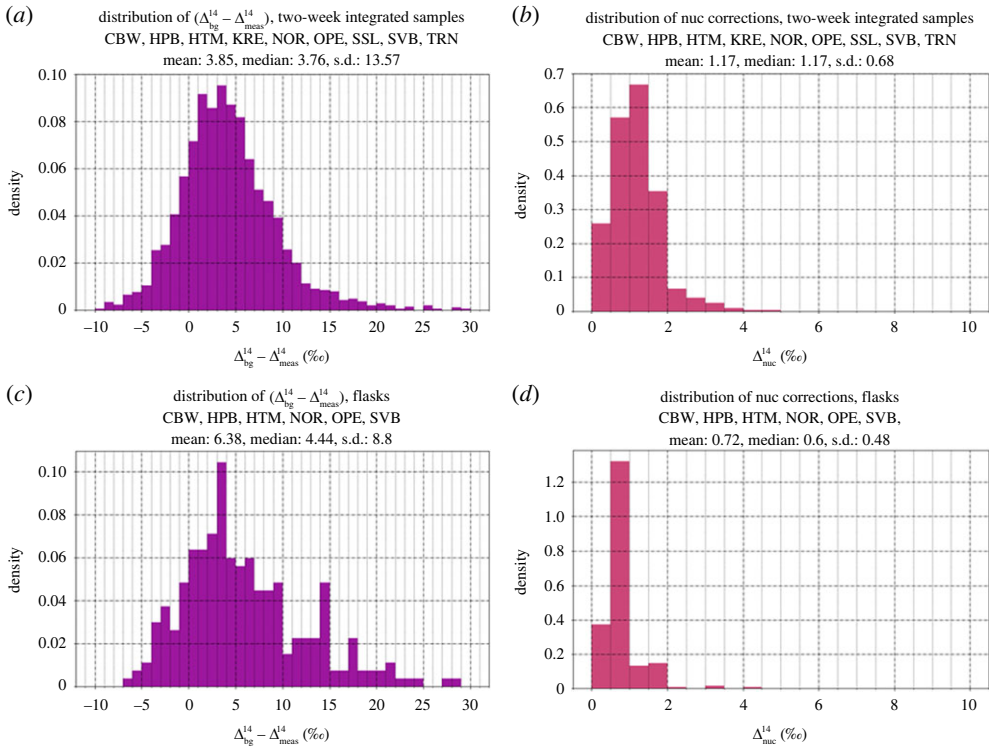

Figure 6. Distribution of observed Δ^{14} signals between reference station (MHD) and ICOS stations ((*a*) for two-week integrated samples and (*c*) for the currently available flask samples). (*b*,*d*) The distributions of the estimated nuclear corrections of the samples.

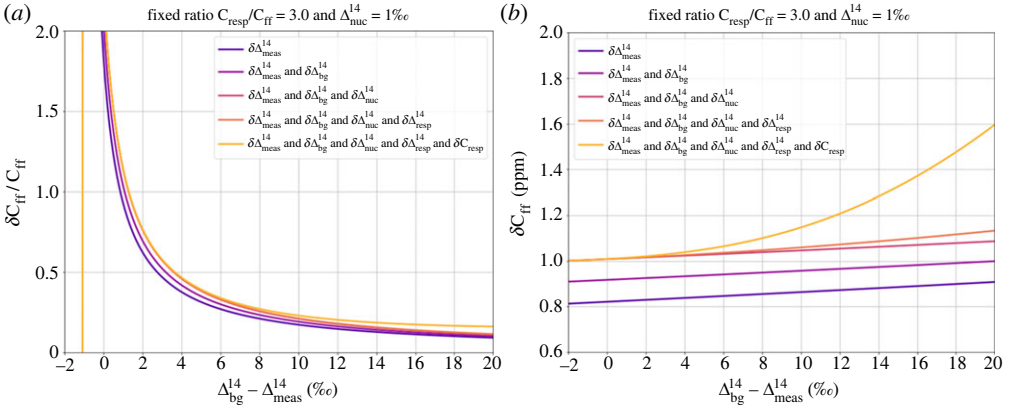

Figure 7. (*a*) Relative uncertainty of $\Delta ffCO_2$ in relation to the observed difference of Δ^{14} between background and station ($\Delta^{14}_{bg} - \Delta^{14}_{meas}$). (*b*) The absolute uncertainty in ppm. Note, the *x*-axis starts at −2 to account for masking effects.

the potential uncertainty of $ffCO_2$ masking by ^{14}C-enriched soil respiration is non-negligible and potentially of similar magnitude as the uncertainty of the contamination from nuclear installations, if the respiration CO_2 is significantly ^{14}C-enriched compared with that of the ambient atmosphere.

Downloaded from https://royalsocietypublishing.org/ on 10 October 2023

4. Discussion and conclusion

The property of fossil emissions being free from ^{14}C makes $\Delta^{14}CO_2$ a unique and direct tracer for the fossil share in regional CO_2 excess compared with a (clean air) background. However, this method, called here the regional isotope budget approach, also has its challenges and uncertainties. In this study, we revisited the assumptions made to address these various challenges and gave an overall uncertainty of the ^{14}C-based $\Delta ffCO_2$ estimates so that those could be used in atmospheric inversion modelling to verify or evaluate fossil fuel emissions. In the following, we will summarize and discuss our main findings.

The first and most important decision is the choice of the background site, as the $\Delta^{14}CO_2$ difference between observation and background site directly determines the $\Delta ffCO_2$ concentrations. In general, the background site should be chosen to suit the target area of the $ffCO_2$ emission estimates. For example, if the emissions of a city are to be sampled, it might be convenient to measure the signals from the city downwind and to use a regional or local background station upwind of the city (e.g. [14]). In our study, we wanted to select a background site for a station network like ICOS that covers wide parts of the European continent. If the $\Delta ffCO_2$ estimates derived with the regional isotope budget approach shall be used as a constraint in an inversion modelling framework to evaluate the fossil fuel emissions, the used background site has to be representative for all boundaries of the targeted domain. Otherwise, $\Delta ffCO_2$ signals originating from outside the domain would be distributed within the domain. For the European example, STILT back-trajectories suggest that the entire European domain is dominated by westerly winds in about two-thirds of all situations. Therefore, we chose MHD, located on the west coast of Ireland, as our background station. To construct a background $\Delta^{14}CO_2$ curve, we calculated a smooth fit through the integrated $\Delta^{14}CO_2$ observations of MHD and estimated its construction uncertainty to be less than 1‰. However, the clean Atlantic air background from MHD might be less representative for potentially slightly polluted continental air masses with non-western origin, which are expected to occur in about one-third of all situations. The lack of representativeness of the MHD reference for these situations induces a bias and an additional uncertainty to the $\Delta ffCO_2$ estimates. We used the global TM3 model [36] and switched off the emissions from the European target area to estimate this representativeness bias and additional uncertainty. The bias depends on the distance between the observation site and the boundaries of the target area, as it affects the dilution of the background signal from the boundaries to the observation site. This means that potential observation sites close to the, e.g. eastern boundary of the target domain, can show substantial biases for situations when they are affected by CO_2 plumes from outside the target region. Therefore, the $\Delta ffCO_2$ estimates from such sites should be corrected for those biases if the $\Delta ffCO_2$ observations are to be used in inverse models to evaluate $ffCO_2$ emissions. Concerning the current ICOS atmosphere stations, these plumes from outside the European domain are typically well mixed when they arrive at the observation site; here we expect mean biases of order 0.1 ppm. Therefore, we think that it is appropriate to use MHD as a single background site for the observation sites in Central Europe and for all wind conditions. Furthermore, we recommend to not exclude data under easterly wind conditions as this could lead to sampling biases if the $\Delta ffCO_2$ estimates are used in an atmospheric transport inversion to optimize $ffCO_2$ emissions. However, the variability in the bias induces a representativeness uncertainty of the MHD reference, which must be added quadratically to the MHD background fit uncertainty. This representativeness uncertainty depends also on the sample type. For Křešín (KRE), which is an eastern ICOS site in Central Europe and therefore expected to be most influenced by a false representation of the eastern boundary, the standard deviation of the bias amounts to 0.12 ppm for two-week integrated samples and 0.28 ppm for potential midday flasks; these could have a bias of up to 2 ppm. The overall background $\Delta^{14}CO_2$ uncertainty (0.9‰ for two-week integrated samples and 1.0‰ for flasks), i.e. the combination of the MHD fit and representativeness uncertainties, together with the measurement uncertainty of the $\Delta^{14}CO_2$ signals at the monitoring sites (*ca* 2‰), account for *ca* 0.9–1.0 ppm uncertainty of the $\Delta ffCO_2$ estimates for typical signals observed at ICOS sites (table 2).

Downloaded from https://royalsocietypublishing.org/ on 10 October 2023

Table 2. Contributions to the overall $\Delta ffCO_2$ uncertainty. The shown uncertainties are representative of a range of ($\Delta^{14}_{bg} - \Delta^{14}_{meas}$) differences from −2 to 20‰, which covers most of the observed range in figure 6. The uncertainty contribution of a certain parameter is the increase in the $\Delta ffCO_2$ uncertainty if the uncertainty of this parameter is (quadratically) added to the $\Delta ffCO_2$ uncertainty, which was caused by the previous parameters (in the rows above this certain parameter).

parameter	contribution to overall $\Delta ffCO_2$ uncertainty	parameter value ± uncertainty
Δ^{14}_{meas}	(0.8–0.9) ppm	± 2‰
Δ^{14}_{bg}	0.1 ppm	(3 ± 1)‰
Δ^{14}_{nuc}	0.1 ppm [0.3 ppm]	(1 ± 1)‰ [(2 ± 2)‰]
Δ^{14}_{resp}	(0–0.05) ppm	(25 ± 12)‰
C_{resp}/C_{ff}	(0–0.5) ppm	3 ± 3
C_{bg}	$\sim 10^{-4}$ ppm	(410 ± 1) ppm
C_{meas}	$\sim 10^{-9}$ ppm	(420 ± 0.1) ppm

In Europe, with more than 170 in-operation reactors and two reprocessing plants [41], the nuclear contamination of the $\Delta^{14}CO_2$ samples is a serious problem. The median nuclear contamination at the ICOS sites accounts for about 30% (for day-and-night integrated samples) and almost 15% (for flasks that are collected during midday integrated over 1 h) of the median $\Delta^{14}CO_2$ depletion compared with the MHD reference. This would roughly result in a 25% and 15%, respectively, underestimation of the $\Delta ffCO_2$ estimates if no correction is applied. Therefore, we strongly recommend correcting the $\Delta ffCO_2$ estimates for nuclear contaminations, especially for sites with small signals or substantial influence from nuclear facilities. The uncertainty for the nuclear contaminations originates from the transport model uncertainty as well as the uncertainty of the nuclear $^{14}CO_2$ emissions. The transport model uncertainty depends on the sample type and the distance to the nuclear facilities. On the one hand, the nuclear corrections might be more reliable for integrated samples than for flasks as it is less relevant when exactly the plume of a nuclear point source hits the observation site. On the other hand, integrated samples include also night-time situations when transport models show typically poorer performance. The uncertainty of the nuclear emissions is mainly based on the strong temporal variability of the emissions [30,42], which we could not consider as we only had access to the officially reported annual mean $^{14}CO_2$ emissions. Therefore, we assumed an uncertainty of 100% for the nuclear corrections. This increases the overall uncertainty of the nuclear corrected $\Delta ffCO_2$ estimates by about 0.1 ppm for a typical nuclear contamination of 1‰. Overall, and particularly for flask sampling, we suggest calculating near-real time (or even better forecast) back-trajectories or footprints so that sampling during situations with potentially large nuclear influences can be avoided.

Soil respiration CO_2 is expected to be a few tens of ‰ enriched in $\Delta^{14}CO_2$ compared with atmospheric CO_2, since it was initially fixed by plants during higher atmospheric $\Delta^{14}CO_2$ levels after the atmospheric nuclear bomb testing. Therefore, also respiration CO_2 may lead to masking part of the $\Delta ffCO_2$ signal, depending on the $\Delta^{14}CO_2$ difference between respired and atmospheric CO_2 and the relative amount of respired CO_2. For typical winter C_{resp}/C_{ff} ratios of 1 (figure 9), the $\Delta ffCO_2$ masking is less than 5% if the respiration $\Delta^{14}CO_2$ signature is enriched by less than 40‰ compared with the ambient $\Delta^{14}CO_2$. However, this masking effect can easily increase for a larger relative share of respiration CO_2, e.g. during summer, and with higher soil respiration $\Delta^{14}CO_2$ signatures. For a typical summer C_{resp}/C_{ff} ratio of 6 at ICOS sites, the $\Delta ffCO_2$ masking reaches already almost 20% for a 40‰ $\Delta^{14}CO_2$ enrichment in the respired CO_2. Therefore, the correction for soil respiration is especially important for sites with low $ffCO_2$ signals and strong biosphere influence, which might be the case for many ICOS sites. The respiration CO_2 component in the ambient CO_2 concentration is hard to estimate, particularly during the day when photosynthesis is active. In these situations, a vegetation model in combination with an

Downloaded from https://royalsocietypublishing.org/ on 10 October 2023

atmospheric transport model is needed. Therefore, we assume an uncertainty of 100% for the respiration CO_2. Moreover, we estimated the uncertainty of the respiration $\Delta^{14}CO_2$ signature to 50% of the $\Delta^{14}CO_2$ enrichment compared with the ambient $\Delta^{14}CO_2$. With those uncertainty assumptions, we expect the contribution of the uncertainty of the biosphere correction to the overall $\Delta ffCO_2$ uncertainty to be smaller than 0.5 ppm for typical ICOS sites.

In this study, we also investigated the effect, if the $\Delta^{14}CO_2$ signature of the photosynthetically absorbed CO_2 is approximated with the ambient air $\Delta^{14}CO_2$ at the measurement site (see equation (2.3)) or, alternatively, with the background $\Delta^{14}CO_2$ observations (see equation (2.4)). It turns out that the relative bias in the $\Delta ffCO_2$ estimates caused by these two different approximations is typically restricted to a few per cent only. The choice between equation (2.3) or equation (2.4) to calculate the $\Delta ffCO_2$ concentrations may also depend on the availability of the required measurements. For example, equation (2.4) requires CO_2 concentration data at the observation site. However, in some cases, the CO_2 concentration at the observation site is not known, e.g. if the $\Delta ffCO_2$ is based on $\Delta^{14}C$ from plant material. For such cases, equation (2.3) might be more useful, as its major term depends on the background CO_2 concentration C_{bg} instead of C_{meas}. However, C_{meas} is also needed in the nuclear correction term (second term of equation (2.3)). We, therefore, investigated the bias if C_{meas} is replaced by C_{bg} in equation (2.3). Obviously, it depends on the CO_2 concentration difference between C_{meas} and C_{bg} and the magnitude of the nuclear contamination. Even if the nuclear contamination is of the order of the Δ^{14} difference between measurement and background site, this bias will still be below 5% for CO_2 differences ($C_{meas} - C_{bg}$) of up to 40 ppm. Thus, this effect is much smaller compared with the bias introduced by neglecting the nuclear correction itself.

Overall, this study shows that the largest single uncertainty contribution to $\Delta ffCO_2$ estimates still comes from the limited precision in $\Delta^{14}CO_2$ analyses if the potential biases due to nuclear contamination or biosphere respiration are corrected for. Even a $\Delta^{14}CO_2$ measurement uncertainty of 1‰ would still make up a substantial contribution to the overall $\Delta ffCO_2$ uncertainty for typical ($\Delta^{14}_{bg} - \Delta^{14}_{meas}$) gradients at ICOS sites and assumed nuclear Δ^{14}_{nuc} contributions of 1‰. This means that about every second (or third) integrated sample from the ICOS network would yield a $\Delta ffCO_2$ uncertainty larger than 50% for an assumed 2‰ (or 1‰) $\Delta^{14}CO_2$ measurement uncertainty. These large relative $\Delta ffCO_2$ uncertainties can be explained by the small ($\Delta^{14}_{bg} - \Delta^{14}_{meas}$) gradients at the remote ICOS sites. Therefore, the regional isotope budget approach is best suited in polluted areas with large Δ^{14}_{meas} depletions due to fossil CO_2 emissions. In such cases, the regional isotope budget approach is also relatively less sensitive to possible representativeness biases in Δ^{14}_{bg}. If the transport-driven variability in the $\Delta ffCO_2$ estimates can be reproduced by an atmospheric transport model, the $\Delta ffCO_2$ observations can be used in inversion frameworks to estimate $ffCO_2$ emissions. Graven *et al*. [18] used ^{14}C-based $\Delta ffCO_2$ observations from nine urban and non-urban sites in California to investigate the $ffCO_2$ surface fluxes with a Bayesian inversion framework based on Fischer *et al*. [43]. They could show that their estimates for the total in-state emissions are consistent with bottom-up estimates. Thus, it would also be interesting to investigate if the $\Delta ffCO_2$ observations from the ICOS sites can be used to estimate the $ffCO_2$ emissions in Europe. Indeed, the signal-to-noise constraints that limit the $\Delta ffCO_2$ detection at remote sites might not limit the inverse problem in the same way. Thus, the large and growing number of samples from distributed ICOS sites with small but persistent $\Delta ffCO_2$ signals may provide meaningful adjustments of the $ffCO_2$ surface fluxes in Central Europe. An alternative approach to investigate $ffCO_2$ emissions is the dual-tracer inversion, which uses the CO_2 and $\Delta^{14}CO_2$ observations directly. This approach has already successfully been applied in the US by Basu *et al*. [10]. The authors used the CO_2 and $\Delta^{14}CO_2$ observations from the NOAA station network in North America and showed that the estimated US national total $ffCO_2$ emissions for 2010 are significantly larger than reported by bottom-up inventories. Undoubtedly, this dual-tracer inversion approach should also be implemented in Europe to take advantage of the ICOS observation network. Ideally, the results of the $ffCO_2$ inversion and the dual-tracer inversion would then converge within their individual uncertainty margins.

Downloaded from https://royalsocietypublishing.org/ on 10 October 2023

Certainly, a big challenge in Europe is the large number of nuclear power plants [29], which affect both, the regional isotope budget approach, and the dual-tracer inversion approach. Thus, there is an urgent need for temporally highly resolved (i.e. at least monthly or weekly) $^{14}CO_2$ emissions data from nuclear facilities in Europe, so that reliable and un-biased $ffCO_2$ emission estimates can be deduced. In other parts of the world with a much lower spatial density of nuclear installations this 'nuclear problem' seems to be less prominent than in Europe. However, we showed that the biosphere respiration could lead to similar biases as the nuclear contaminations if not properly taken into account. In other rural regions of the world the respiration Δ^{14}_{resp} might be different, depending on climate and vegetation types. This must be considered, so that $\Delta ffCO_2$ concentrations can be estimated bias-free. But also, the dual-tracer inversion requires a reliable *a priori* representation of the Δ^{14}_{resp} signature.

Finally, we showed that a marine site located at the western edge of the European target region is an appropriate background site for calculating $\Delta ffCO_2$ estimates for sites in Central Europe. Similarly, Graven *et al*. [18] used measurements from three coastal sites in California to construct a $\Delta^{14}CO_2$ background for observation sites in California. Zhou *et al*. [17] defined the Qixianling Mountain, which is located on the Hainan Island in the south of China as a background to estimate $\Delta ffCO_2$ concentrations for 15 Chinese cities. To conclude, if the $\Delta^{14}C$ observations of a single site are used to estimate $\Delta ffCO_2$ concentrations for an observation network, a potential background representativeness bias and uncertainty should be investigated by either comparing the Δ^{14}_{bg} values with observations from other potential background sites or estimating the representativeness bias via model simulations as in the present study.

Data accessibility. This article has no additional data. Radiocarbon observations from the ICOS sites can be downloaded from the ICOS Carbon Portal (https://www.icos-cp.eu/, last access: 29 August 2023).

Authors' contributions. F.M.: conceptualization, formal analysis, investigation, methodology, writing—original draft; I.L.: conceptualization, formal analysis, investigation, methodology, writing—original draft; M.G.: conceptualization, investigation, methodology, writing—review and editing; C.R.: conceptualization, investigation, methodology, writing—review and editing; S.H.: conceptualization, investigation, methodology, writing—review and editing.

All authors gave final approval for publication and agreed to be held accountable for the work performed therein.

Conflict of interest declaration. We declare we have no competing interests.

Funding. The ICOS-CRL is funded by the German Federal Ministry for Digital and Transport. F.M. was funded by the VERIFY Project (EC grant no. 776810).

Acknowledgements. We are grateful to Sabine Kühr, Eva Gier, Julian Della Coletta and the whole staff of the ICOS Central Radiocarbon Laboratory (CRL) as well as the ICOS Atmosphere stations for collecting and analysing the integrated and flask samples. Moreover, we like to thank Ida Storm and the members of the ICOS Carbon Portal for developing and providing a Jupyter notebook for the estimation of nuclear $^{14}CO_2$ contaminations at the ICOS stations.

Appendix A

A.1. Nuclear contaminations and their uncertainties

We used the $^{14}CO_2$ emissions from the European Commission RAdioactive Discharges Database (RADD) where the member states of the European Union report their annual nuclear emissions [44]. For some facilities, only the total ^{14}C emission but not the $^{14}CO_2$ emission is reported. In these cases, we assume that pressurized water reactors (PWRs) emit 28% of the ^{14}C as $^{14}CO_2$ and that all other reactor types emit all ^{14}C as $^{14}CO_2$ according to Zazzeri *et al*. [45] and Graven & Gruber [29]. Since the Belgian facilities are missing in the RADD database, we used the energy consumption data from the International Atomic Energy Agency-Power Reactor Information System (IAEA-PRIS, available at: https://pris.iaea.org/PRIS/CountryStatistics/CountryDetails.aspx?current=BE, last access: 5 October 2022) and multiplying a factor of 0.24 TBq/a per GWa for PWRs and 0.51 TBq/a per GWa for boiling water reactors to get the annual ^{14}C emissions (as [45]). For the nuclear facilities in Switzerland the $^{14}CO_2$ emissions were taken from the annual

Downloaded from https://royalsocietypublishing.org/ on 10 October 2023

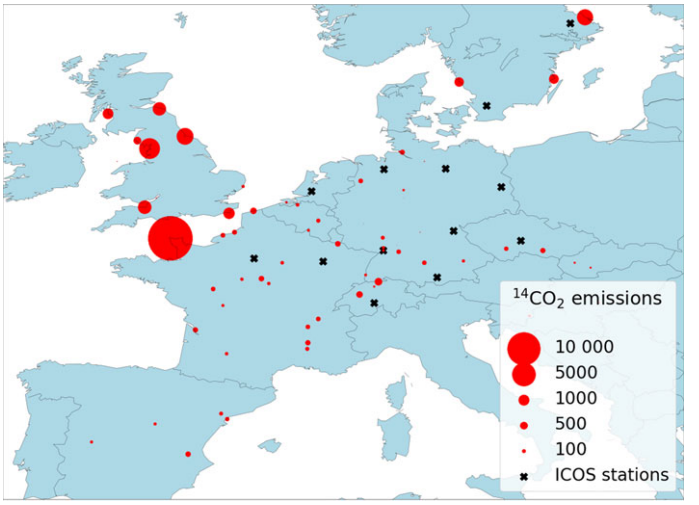

Figure 8. Nuclear $^{14}CO_2$ emissions in Europe (annual means for 2018). The black crosses show the locations of the ICOS class-1 stations. See the text for a description of how this map was created.

Radiological Protection Reports (available at: https://www.ensi.ch/en/documents/document-category/strahlenschutzberichte/, last access: 5 October 2022) authored by the Swiss Federal Nuclear Safety Inspectorate (ENSI). This nuclear $^{14}CO_2$ emission map (figure 8) has been implemented at the ICOS CP.

To calculate the $\Delta^{14}CO_2$ contaminations from nuclear facilities at the observation site (Δ^{14}_{nuc}), we transport the $^{14}CO_2$ emissions with the STILT model [26]. In STILT, the surface source influence f with units $(\mu mol/mol_{air})/(\mu mol/m^2 s)$ describes the sensitivity to emissions from surface grid cells (x_i, y_j) in the footprint of the station. As the nuclear $^{14}CO_2$ emissions Q are given in units $Bq/(m^2 s)$, the mapping of those emissions with the surface source influence f yields a nuclear activity $A_S = (Q \circ f)$ in units Bq/mol_{air} ('o' indicates the element-wise multiplication of each surface influence grid cell (x_i, y_j) with its corresponding flux $Q(x_i, y_j)$ and the subsequent sum over all grid cells). Equation (A 1) gives the definition of the Δ-notation according to Stuiver & Pollach [24] and equation (A 2) the Δ^{14}_{nuc}:

$$\Delta^{14}CO_2 = \left(\frac{A_{SN}}{A_{abs}} - 1\right) \cdot 1000‰ \approx \left(\frac{0.968 \cdot A_S}{A_{abs}} - 1\right) \cdot 1000‰ \tag{A 1}$$

and

$$\Delta^{14}_{nuc} = \frac{0.968 \cdot (Q \circ f)}{C_{meas} \cdot M_C \cdot A_{abs}} \cdot 1000‰. \tag{A 2}$$

Here, we assume a constant atmospheric $\delta^{13}C$–CO_2 value of $-9‰$ and use the standard activity A_{abs} of 0.226 Bq/gC ('gC' means gram carbon). To get the sample activity in the same units as the standard activity, we have to divide the sample activity by the product of the CO_2 concentration at the measurement site C_{meas} and the molar mass of carbon M_C. Since the RADD nuclear emissions are reported only on an annual basis, we assume constant emissions throughout the year. This procedure of mapping the RADD $^{14}CO_2$ emissions with modelled surface source influences has been implemented in the radiocarbon Jupyter notebook offered by the ICOS Carbon Portal. The surface source influence fields are available for all ICOS sites on a three-hourly resolution and were generated with 0.25° resolution meteorological data from the European Center for Medium-Range Weather Forecasts (ECMWF). Since the nuclear emissions are released from stacks with a height of typically above 100 m, using the standard STILT approach that can transport only surface emissions, may overestimate $^{14}CO_2$ activity concentrations during stable (night-time) conditions if the nuclear installations are located closer

Downloaded from https://royalsocietypublishing.org/ on 10 October 2023

than *ca* 50 km from the measurement site. For these stations a more sophisticated approach introduced by Maier *et al*. [27] should be applied. In the current study we did, however, only use the standard surface influence approach and the distribution of Δ^{14}_{nuc} for integrated samples shown in figure 6*b* may, thus, be slightly biased high for some of the stations (i.e. NOR).

The uncertainty of the transport model is mainly due to the uncertainty of the meteorological input fields and their resolution as well as on the correct representation of the effective emission heights. Kuderer *et al*. [30] showed with the Hybrid Single-Particle Lagrangian Integrated Trajectory (HYSPLIT) model that the mean nuclear contamination from nearby power plants can be more than doubled if the horizontal resolution of the meteorological fields is increased from 0.5° to 2.5°. Therefore, we used high-resolution meteorological fields from ECMWF. Considering these various and difficult-to-quantify sources of uncertainty to calculate Δ^{14}_{nuc}, we chose a simple but justified approach and applied an uncertainty of 100% for all sample types. This allows on the one hand to cover situations with the dominant nuclear $^{14}CO_2$ emissions during the two-week period being twice as high as expected (i.e. the annual average). On the other hand, it considers situations when the model erroneously predicts nuclear influences at the observation site.

A.2. Construction of the MHD Δ^{14}_{bg} background curve

In this study, we use the two-week integrated $\Delta^{14}CO_2$ data from the maritime site MHD (53.33° N, 9.90° W, 5 m a.s.l.) located at the west coast of Ireland to calculate marine background reference curves for all ICOS stations. We applied the curve fitting algorithm from the NOAA to the two-week integrated $\Delta^{14}CO_2$ measurements. A description of the fitting routine can be found at: https://gml.noaa.gov/ccgg/mbl/crvfit/crvfit.html and a Python script is freely available at: https://gml.noaa.gov/aftp/user/thoning/ccgcrv/ (last access: 11 March 2022). We used the following three components of the NOAA curve fitting routine: (i) a polynomial function with three terms (i.e. a quadratic function) to account for the long-term $\Delta^{14}CO_2$ decline, (ii) two harmonics to simulate the annual $\Delta^{14}CO_2$ cycle and (iii) a low-pass filter to the residuals with a long-term cut-off value of 5 years to consider interannual variations. This NOAA fitting routine also provides variances σ^2_{func} and σ^2_{filt} for the function, which is set up by the polynomial terms and the harmonics, and for the low-pass filtering of the residuals, respectively. The total variance σ^2_{fit} of the NOAA fit is then given by the combination of both variances (see https://gml.noaa.gov/ccgg/mbl/crvfit/crvfit.html, equation (A 3)):

$$\sigma^2_{fit} = \sigma^2_{func} + \sigma^2_{filt}. \tag{A 3}$$

The NOAA fitting routine was originally developed for CO_2 concentrations, which can be measured very accurately with uncertainties of typically below 0.1 ppm. So, the ratio between measurement uncertainty and a typical seasonal variation of 20 ppm is only 5‰. That is why the measurement uncertainties of the individual observations are not considered by the NOAA fit. However, in the case of $\Delta^{14}CO_2$ the measurement uncertainty is *ca* 2‰, which is 40% of a typical 5‰ peak-to-peak seasonal $\Delta^{14}CO_2$ variation at background sites. Therefore, we also performed a Monte Carlo approach, to take into account the measurement uncertainties of the individual two-week integrated $\Delta^{14}CO_2$ samples. We draw for each $\Delta^{14}CO_2$ sample a random number from a Gaussian distribution with zero mean and the one-sigma standard deviation given by the respective measurement uncertainty. The initial $\Delta^{14}CO_2$ measurements were then shifted by those random numbers. Afterwards, we calculated the NOAA fitting curve for this configuration. After repeating this procedure 1000 times, we could calculate the standard deviation over all 1000 background curves to get an additional estimate of the average background curve uncertainty.

The NOAA fitting routine yields a standard deviation for Δ^{14}_{bg} of 0.86‰ for the points relative to the background curve, while the standard deviation over the 1000 Monte Carlo realizations was on average only 0.43‰, i.e. half the standard deviation calculated with the NOAA fitting algorithm. This small standard deviation of the Monte Carlo realizations shows that the chosen parameters (i.e. the long-term cut-off value of 5 years) leads to a background curve, which is

Downloaded from https://royalsocietypublishing.org/ on 10 October 2023

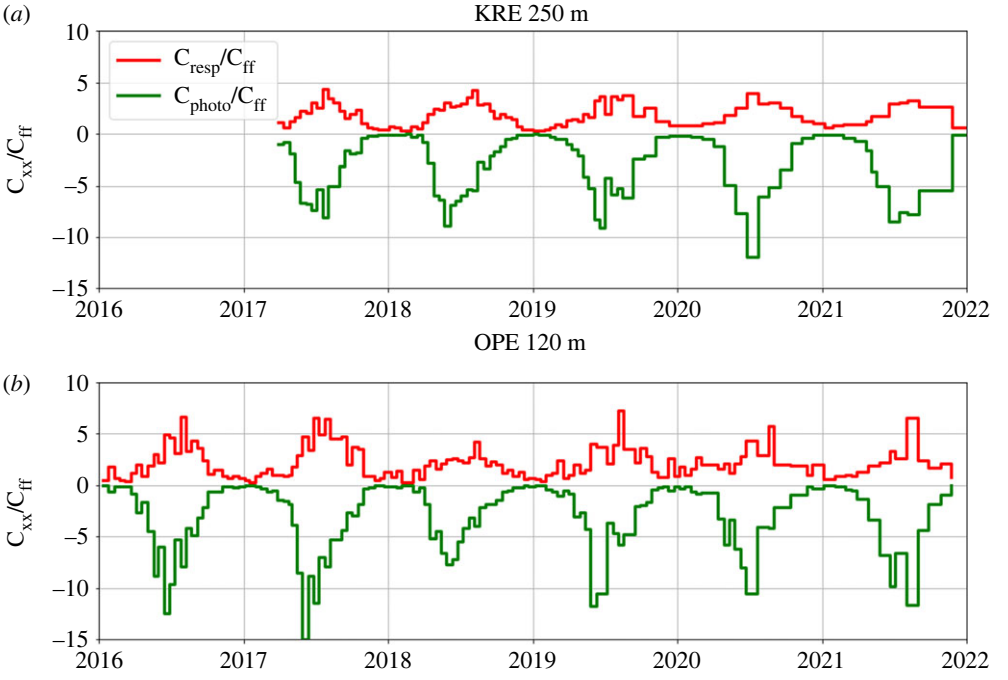

Figure 9. Simulated C_{photo}/C_{ff} (green) and C_{resp}/C_{ff} (red) ratios for the integrated samples collected at the two ICOS sites KRE (*a*) and OPE (*b*).

robust to variations within the one-sigma range of the individual $\Delta^{14}CO_2$ measurements. If we vary the individual $\Delta^{14}CO_2$ measurements within their two-sigma uncertainty range, we get a standard deviation of 0.86‰ over the 1000 Monte Carlo realizations, i.e. the same value as the standard deviation computed with the NOAA algorithm. We also investigated the influence of a different number of polynomials (two or four polynomials instead of three), harmonics (three or four harmonics instead of two) and years for the long-term cut-off value (1 or 3 years instead of 5). These parameter-varied background curves lie all well within the 0.86‰ uncertainty band of the MHD background curve. On average, the deviations are even less than 0.1‰. That is why we will use in the following the 0.86‰ standard deviation as an estimate for the uncertainty of the MHD background $\Delta^{14}CO_2$ curve.

A.3. Modelled C_{resp}/C_{ff} and C_{photo}/C_{ff} ratios for two ICOS sites

Figure 9 shows the modelled C_{photo}/C_{ff} and C_{resp}/C_{ff} ratios for the integrated samples collected at the two ICOS sites Křešín (KRE) in the Czech Republic and Observatoire Pérenne de l'Environnement (OPE) in France between 2016 and 2021. We used VPRM-STILT to simulate the biospheric CO_2 signals and the Emissions Database for Global Atmospheric Research (EDGAR, [46]) and STILT to calculate the C_{ff} contributions. The model results illustrate the expected range of the ratios at typical ICOS sites in Central Europe as well as their seasonal cycle with lower (absolute) ratios in winter compared with summer.

References

1. Friedlingstein P *et al.* 2022 Global Carbon Budget 2021. *Earth Syst. Sci. Data* **14**, 1917–2005. (doi:10.5194/essd-14-1917-2022)

Downloaded from https://royalsocietypublishing.org/ on 10 October 2023

2. Bergamaschi P *et al.* 2018 *Atmospheric monitoring and inverse modelling for verification of greenhouse gas inventories, JRC111789, EUR 29276 EN*. Luxembourg: Publications Office of the European Union. (doi:10.2760/759928)
3. Petrescu AMR *et al.* 2021 The consolidated European synthesis of CH_4 and N_2O emissions for the European Union and United Kingdom: 1990–2017. *Earth Syst. Sci. Data* **13**, 2307–2362. (doi:10.5194/essd-13-2307-2021)
4. Levin I, Münnich KO, Weiss W. 1980 The effect of anthropogenic CO_2 and ^{14}C sources on the distribution of ^{14}C in the atmosphere. *Radiocarbon* **22**, 379–391. (doi:10.1017/S003382220000967X)
5. Levin I, Kromer B, Schmidt M, Sartorius H. 2003 A novel approach for independent budgeting of fossil fuel CO_2 over Europe by $^{14}CO_2$ observations. *Geophys. Res. Lett.* **30**, 2194. (doi:10.1029/2003GL018477)
6. Turnbull JC, Miller JB, Lehman SJ, Tans PP, Sparks RJ, Southon J. 2006 Comparison of $^{14}CO_2$, CO, and SF_6 as tracers for recently added fossil fuel CO_2 in the atmosphere and implications for biological CO_2 exchange. *Geophys. Res. Lett.* **33**, L01817. (doi:10.1029/2005GL024213)
7. Miller JB *et al.* 2012 Linking emissions of fossil fuel CO_2 and other anthropogenic trace gases using atmospheric $^{14}CO_2$. *J. Geophys. Res.* **117**, D08302. (doi:10.1029/2011JD017048)
8. Basu S, Miller JB, Lehman S. 2016 Separation of biospheric and fossil fuel fluxes of CO_2 by atmospheric inversion of CO_2 and $^{14}CO_2$ measurements: observation system simulations. *Atmos. Chem. Phys.* **16**, 5665–5683. (doi:10.5194/acp-16-5665-2016)
9. Wang Y, Broquet G, Ciais P, Chevallier F, Vogel F, Wu L, Yin Y, Wang R, Tao S. 2018 Potential of European $^{14}CO_2$ observation network to estimate the fossil fuel CO_2 emissions via atmospheric inversions. *Atmos. Chem. Phys.* **18**, 4229–4250. (doi:10.5194/acp-18-4229-2018)
10. Basu S, Lehman SJ, Miller JB, Andrews AE, Sweeney C, Gurney KR, Xue X, Southon J, Tans PP. 2020 Estimating US fossil fuel CO_2 emissions from measurements of ^{14}C in atmospheric CO_2. *Proc. Natl Acad. Sci. USA* **117**, 13 300–13 307. (doi:10.1073/pnas.1919032117)
11. Potier E *et al.* 2022 Complementing XCO_2 imagery with ground-based CO_2 and $^{14}CO_2$ measurements to monitor CO_2 emissions from fossil fuels on a regional to local scale. *Atmos. Meas. Tech.* **15**, 5261–5288. (doi:10.5194/amt-15-5261-2022)
12. Levin I, Rödenbeck C. 2008 Can the envisaged reductions of fossil fuel CO_2 emissions be detected by atmospheric observations? *Naturwissenschaften* **95**, 203–208. (doi:10.1007/s00114-007-0313-4)
13. Levin I, Hammer S, Eichelmann E, Vogel F. 2011 Verification of greenhouse gas emission reductions: the prospect of atmospheric monitoring in polluted areas. *Phil. Trans. A Math. Phys. Eng. Sci.* **369**, 1906–1924. (doi:10.1098/rsta.2010.0249)
14. Turnbull J *et al.* 2015 Toward quantification and source sector identification of fossil fuel CO_2 emissions from an urban area: results from the INFLUX experiment. *J. Geophys. Res. Atmos.* **120**, 292–312. (doi:10.1002/2014JD022555)
15. Berhanu TA *et al.* 2017 Estimation of the fossil fuel component in atmospheric CO_2 based on radiocarbon measurements at the Beromünster tall tower, Switzerland. *Atmos. Chem. Phys.* **17**, 10 753–10 766. (doi:10.5194/acp-17-10753-2017)
16. Major I, Haszpra L, Rinyu L, Futó I, Bihari Á, Hammer S, Jull AJT, Molnár M. 2018 Temporal variation of atmospheric fossil and modern CO_2 excess at a Central European rural tower station between 2008 and 2014. *Radiocarbon* **60**, 1285–1299. (doi:10.1017/rdc.2018.79)
17. Zhou W *et al.* 2020 Fossil fuel CO_2 traced by radiocarbon in fifteen Chinese cities. *Sci. Total Environ.* **729**, 138639. (doi:10.1016/j.scitotenv.2020.138639)
18. Graven HD *et al.* 2018 Assessing fossil fuel CO_2 emissions in California using atmospheric observations and models. *Environ. Res. Lett.* **13**, 065007. (doi:10.1088/1748-9326/aabd43)
19. Caldeira K, Rau GH, Duffy PB. 1998 Predicted net efflux of radiocarbon from the ocean and increase in atmospheric radiocarbon content. *Geophys. Res. Lett.* **25**, 3811–3814. (doi:10.1029/1998GL900010)
20. Randerson JT, Enting IG, Schuur EAG, Caldeira K, Fung IY. 2002 Seasonal and latitudinal variability of troposphere $\Delta^{14}CO_2$: post bomb contributions from fossil fuels, oceans, the stratosphere, and the terrestrial biosphere. *Glob. Biogeochem. Cycles* **16**, 1112. (doi:10.1029/2002GB001876)

Downloaded from https://royalsocietypublishing.org/ on 10 October 2023

21. Naegler T, Levin I. 2009 Observation-based global biospheric excess radiocarbon inventory 1963–2005. *J. Geophys. Res.* **114**, D17302. (doi:10.1029/2008JD011100)
22. Levin I *et al.* 2020 A dedicated flask sampling strategy developed for Integrated Carbon Observation System (ICOS) stations based on CO_2 and CO measurements and Stochastic Time-Inverted Lagrangian Transport (STILT) footprint modelling. *Atmos. Chem. Phys.* **20**, 11 161–11 180. (doi:10.5194/acp-20-11161-2020)
23. Heiskanen J *et al.* 2022 The integrated carbon observation system in Europe. *Bull. Am. Meteorol. Soc.* **103**, E855–E872. (doi:10.1175/BAMS-D-19-0364.1)
24. Stuiver M, Polach H. 1977 Discussion reporting of ^{14}C data. *Radiocarbon* **19**, 355–363. (doi:10.1017/S0033822200003672)
25. Tans PP, Berry JA, Keeling RF. 1993 Ocean $^{13}C/^{12}C$ observations: a new window on ocean CO_2 uptake. *Glob. Biogeochem. Cycles* **7**, 353–368. (doi:10.1029/93GB00053)
26. Lin JC, Gerbig C, Wofsy SC, Andrews AE, Daube BC, Davis KJ, Grainger CA. 2003 A near-field tool for simulating the upstream influence of atmospheric observations: the Stochastic Time-Inverted Lagrangian Transport (STILT) model. *J. Geophys. Res.* **108**, 4493. (doi:10.1029/2002JD003161)
27. Maier F, Gerbig C, Levin I, Super I, Marshall J, Hammer S. 2022 Effects of point source emission heights in WRF–STILT: a step towards exploiting nocturnal observations in models. *Geosci. Model Dev.* **15**, 5391–5406. (doi:10.5194/gmd-15-5391-2022)
28. Lingenfelter RE. 1963 Production of carbon 14 by cosmic-ray neutrons. *Rev. Geophys.* **1**, 35–55. (doi:10.1029/RG001i001p00035)
29. Graven HD, Gruber N. 2011 Continental-scale enrichment of atmospheric $^{14}CO_2$ from the nuclear power industry: potential impact on the estimation of fossil fuel-derived CO_2. *Atmos. Chem. Phys.* **11**, 12 339–12 349. (doi:10.5194/acp-11-12339-2011)
30. Kuderer M, Hammer S, Levin I. 2018 The influence of $^{14}CO_2$ releases from regional nuclear facilities at the Heidelberg $^{14}CO_2$ sampling site (1986–2014). *Atmos. Chem. Phys.* **18**, 7951–7959. (doi:10.5194/acp-18-7951-2018)
31. Naegler T, Levin I. 2009 Biosphere-atmosphere gross carbon exchange flux and the $^{\Delta 13}CO_2$ and $\Delta^{14}CO_2$ disequilibria constrained by the biospheric excess radiocarbon inventory. *J. Geophys. Res.* **114**, D17303. (doi:10.1029/2008JD011116)
32. Palonen V, Pumpanen J, Kulmala L, Levin I, Heinonsalo J, Vesala T. 2018 Seasonal and diurnal variations in atmospheric and soil air $^{14}CO_2$ in a boreal scots pine forest. *Radiocarbon* **60**, 283–297. (doi:10.1017/RDC.2017.95)
33. Chanca I. 2022 Theoretical and experimental approaches using $\Delta^{14}C$ for estimating system diagnostic times in the central Amazon rainforest. PhD Thesis, Instituto de Física, Universidade Federal Fluminense.
34. Mahadevan P *et al.* 2008 A satellite-based biosphere parameterization for net ecosystem CO_2 exchange: Vegetation Photosynthesis and Respiration Model (VPRM). *Glob. Biogeochem. Cycles* **22**, GB2005. (doi:10.1029/2006GB002735)
35. ICOS RI. 2020 ICOS Atmosphere Station Specifications V2.0 edited by: Laurent, O., ICOS ERIC. (doi:10.18160/GK28-2188)
36. Heimann M, Körner S. 2003 The Global Atmospheric Tracer Model TM3, Model Description and User's Manual Release 3.8a, Tech. Rep. 5. Jena, Germany: Max Planck Institute for Biogeochemistry (MPI-BGC).
37. Jones MW *et al.* 2022 Code for: Gridded fossil CO_2 emissions and related O_2 combustion consistent with national inventories 1959–2021 (GCP-GridFEDv2022.2) [Data set]. *Zenodo*. (doi:10.5281/zenodo.7016360)
38. Levin I, Hammer S, Kromer B, Preunkert S, Weller R, Worthy D. 2021 Radiocarbon in global tropospheric carbon dioxide. *Radiocarbon* **64**, 781–791. (doi:10.1017/RDC.2021.102)
39. Hammer S *et al.* 2017 Compatibility of atmospheric $^{14}CO_2$ measurements: comparing the Heidelberg low-level counting facility to international accelerator mass spectrometry (AMS) laboratories. *Radiocarbon* **59**, 875–883. (doi:10.1017/RDC.2016.62)
40. Thoning KW, Tans PP, Komhyr WD. 1989 Atmospheric carbon dioxide at Mauna Loa Observatory: 2. Analysis of the NOAA GMCC data, 1974–1985. *J. Geophys. Res.* **94**, 8549–8565. (doi:10.1029/JD094iD06p08549)
41. IAEA-PRIS. 2022 International Atomic Energy Agency - Power Reactor Information System. See https://pris.iaea.org/pris/home.aspx (last access: 5 October).

42. Varga T, Major I, Gergely V, Lencsés A, Bujtás T, Jull AJT, Veres M, Molnár M. 2021 Radiocarbon in the atmospheric gases and PM10 aerosol around the Paks Nuclear Power Plant, Hungary. *J. Environ. Radioact.* **237**, 106670. (doi:10.1016/j.jenvrad.2021.106670)
43. Fischer ML *et al.* 2017 Simulating estimation of California fossil fuel and biosphere carbon dioxide exchanges combining in situ tower and satellite column observations. *J. Geophys. Res. Atmos.* **122**, 3653–3671. (doi:10.1002/2016JD025617)
44. RADD. 2022 European Commission RAdioactive Discharges Database. See https://europa.eu/radd/query.dox?pageID=Query (last access: 11 March 2022).
45. Zazzeri G, Acuña Yeomans E, Graven HD. 2018 Global and regional emissions of radiocarbon from nuclear power plants from 1972 to 2016. *Radiocarbon* **60**, 1067–1081. (doi:10.1017/RDC.2018.42)
46. Janssens-Maenhout G *et al.* 2019 EDGAR v4.3.2 Global Atlas of the three major greenhouse gas emissions for the period 1970–2012. *Earth Syst. Sci. Data* **11**, 959–1002. (doi:10.5194/essd-11-959-2019)

Downloaded from https://royalsocietypublishing.org/ on 10 October 2023